Blue–green color-tunable emissions in novel transparent Sr_2LuF_7:Eu/Tb glass-ceramics for WLEDs

Xiaoman Li (李晓曼)[1,2,*], Shaoshuai Zhou (周少帅)[1], Rongfei Wei (魏荣妃)[3], Xueyun Liu (刘雪云)[4], Bingqiang Cao (曹丙强)[1,], and Hai Guo (郭 海)[3]**

[1]*School of Physics and Physical Engineering, Shandong Provincial Key Laboratory of Laser Polarization and Information Technology, Qufu Normal University, Qufu 273165, China*

[2]*State Key Laboratory of Luminescent Materials and Devices, South China University of Technology, Guangzhou 510640, China*

[3]*Department of Physics, Zhejiang Normal University, Jinhua 321004, China*

[4]*Laboratory of Infrared Materials and Devices, Advanced Technology Research Institute, Ningbo University, Ningbo 315211, China*

**Corresponding author: lxmwyk668@qfnu.edu.cn; **corresponding author: caobq@qfnu.edu.cn*

Received December 1, 2019; accepted January 10, 2020; posted online April 29, 2020

To introduce ordered nano-structures inside a transparent amorphous matrix with superior optical and mechanical properties bears scientific and technological importance, yet limited success has been achieved. Here, via simple melting-quenching and subsequent thermal activation, we report the successful preparation of transparent nano-structured glass-ceramics embedded in Sr_2LuF_7 nano-crystals (~26 nm), as evidenced by X-ray diffraction, transmission electron microscopy (TEM), and high resolution TEM. The successful incorporation of dopants into formed Sr_2LuF_7 nano-crystals with low phonon energy results in highly tunable blue–green photoemission, which depends on excitation wavelength, dopant type, and temperature. We found that Eu^{3+} and Eu^{2+} ions co-exist in this hybrid optical material, accompanied by the broadband blue emission of Eu^{2+} and sharp red emissions of Eu^{3+}. A series of optical characterizations are summoned, including emission/excitation spectrum and decay curve measurement, to reveal the reduction mechanism of Eu^{3+} to Eu^{2+}. Furthermore, near green–white photoemission is achieved via the enrichment of Tb^{3+}/Eu^{3+} into crystallized Sr_2LuF_7 nano-crystals. The temperature-dependent visible photoemission reveals thermal activation energy increases with the precipitation of Sr_2LuF_7 nano-crystals in a glass matrix, suggesting better thermal stability of glass-ceramics than precursor glasses. These results could not only deepen the understanding of glass-ceramics but also indicate the promising potential of Eu^{3+}/Tb^{3+}-ions-doped Sr_2LuF_7 glass-ceramics for UV pumped white light emitting diodes (WLEDs) with good thermal stability.

Keywords: glass-ceramics; Sr_2LuF_7 nano-crystals; WLED; luminescent materials.

doi: 10.3788/COL202018.051601.

White light emitting diodes (WLEDs), on account of their energy-saving and environment-friendly features, present diverse applications in general lighting, equipment indicators, backlights and car headlights, etc.[1–7]. In particular, high power ultraviolet (UV) pumped WLEDs are attracting much attention due to un-matched advantages, including high color rendering index and low color temperature[8,9]. However, resins are usually used to package phosphors when we prepare WLEDs, and the inherently short-lived properties of organic compounds have severely limited the long-term use of WLEDs, especially under the action of high power. The aging of the resins also inevitably causes color drift, decline in efficiency, etc.[10].

As an alternative, inorganic oxide glasses offer a promising route for the realization of WLEDs with excellent stability, low cost, and an organic resin free assembly process. So far, typical investigations have been conducted in doped bulk oxide glasses to obtain excellent optical performance for WLEDs[11–13]. Yet, oxide glasses usually bear higher phonon energy, which limits the probability of radiative transitions, resulting in weak emission intensity[14]. Although fluoride glasses present a low phonon energy, the improved emission efficiency is often at the expense of mechanical properties, especially compared to that of oxide glasses[15].

Interestingly, by introducing ordered fluoride nano-crystals inside transparent amorphous oxide glasses, superior optical performance of fluoride and mechanical properties of oxide glass can be preserved at the same time[16,17]. The doped rare earth ions will be incorporated into formed fluoride nano-crystals with low phonon energy, resulting in improved optical properties compared to parent glasses[13,17–24]. Furthermore, the protection of oxide glass networks to the active fluoride nano-crystals can effectively isolate the outside air and the corrosion of moisture to the fluoride nano-crystals, so as to preserve the excellent mechanical properties of oxide glasses[25–27]. Thus, rare earth ions activated oxyfluoride glass-ceramics[28–31] present huge potential in high power WLEDs.

Except for the selection of host, suitable dopants are essential to achieving high performance oxyfluoride glass-ceramics. Eu^{3+} ions with orange–red emission have been

Table 1. Compositions of Glasses Samples (in mol%)

Samples	Host	Eu	Tb
PGEu/GCEu	$SiO_2 - Al_2O_3 - SrF_2 - LuF_3$	$0.5EuF_3$	0
PGEuTb/GCEuTb	$SiO_2 - Al_2O_3 - SrF_2 - LuF_3$	$0.5EuF_3$	$0.5TbF_3$
PGTb/GCTb	$SiO_2 - Al_2O_3 - SrF_2 - LuF_3$	0	$0.5TbF_3$

well accepted as excellent emitters and optical probes due to the sensitive features to surrounding environment[32], while Eu^{2+} ions in glasses normally present a broad emission covering the blue–green spectral region[33]. Therefore, white emission can be achieved by using the red emission of Eu^{3+} with the broad blue emission of Eu^{2+} in appropriately designed glass-ceramics[34,35]. Single phased glass-ceramics with dual emission from Eu^{2+}/Eu^{3+} should be promising in WLEDs; yet, they are rarely reported due to lack of a proper glass-ceramics host for the co-existence of Eu^{3+} and Eu^{2+}.

Here, novel Sr_2LuF_7 nano-crystals were successfully prepared *in situ* via thermal activation inside alumino-silicate glass-ceramics. Under a flexible excitation wavelength, Sr_2LuF_7 glass-ceramics could present color-tunable photoemission by using the merits of the dual emission feature of Eu^{3+} and Eu^{2+}, which cover the whole visible emission range, presenting great potential in WLEDs. The Eu/Tb co-doped glass-ceramics were also prepared to adjust the emission color. The structure and luminescence properties have been systematically studied based on detailed optical and structural characterization. Our results indicate that rare-earth-ion-doped Sr_2LuF_7 glass-ceramics with tunable emission and excellent stability could be excellent candidates for plant lighting or WLEDs.

Via the melting-quenching method, samples with a nominal composition (Table 1) were prepared. SiO_2, Al_2O_3, SrF_2, NaF (A.R.), and high purity LuF_3, EuF_3, and TbF_3 (99.99%) were chosen as raw materials. Typically, 25 g of well mixed raw materials were melted in a crucible (1550°C for 1 h) and quenched in a plate to form a solid bulk glass sample, that is precursor glass (PG), which is denoted as PGEu, PGTb, and PGEuTb. All PGs were isothermal treated (750°C for 5 h) to form corresponding glass-ceramics (GC) samples (labeled as GCEu, GCTb, and GCEuTb, respectively). For further measurement, these PG and GC samples were optically polished.

X-ray diffraction (XRD) patterns were obtained via a Philips X'Pert PRO SUPER XRD apparatus. The microstructure was evaluated by JEM-2010 transmission electron microscopy (TEM) (JOEL Ltd.). Transmittance of PG and GC samples was recorded on a U-3900 UV-visible (UV-VIS) spectrophotometer (Hitachi). Optical characterizations were done on an Edinburgh FS920 fluorescence spectrometer. Temperature control of the sample in the temperature-dependent spectra was realized through heat conduction with a copper plate, whose temperature was controlled using a heating tube and a temperature controller (OMRON E5CC-800).

Figure 1(a) demonstrates the XRD patterns of glass samples including PGEuTb, GCEu, GCTb, and GCEuTb. The standard diffraction data for tetragonal Sr_2LuF_7 are also given for comparison (JCPDS card No. 39-0926). All PG samples are amorphous, and no diffraction peaks are typically seen for PGEuTb. After thermal activation, sharp diffraction peaks of all GC samples corresponding to tetragonal Sr_2LuF_7 emerge, indicating that GC samples are crystallized during thermal treatment. Moreover, different dopants do not cause phase changes. The crystalline size D can be acquired by the following Scherer's equation[36], and it is about 28 nm in diameter for GC samples:

$$D = k\lambda/\beta\cos\theta. \tag{1}$$

As presented in the transmittance spectra of PGEu, GCEu, PGEuTb, and GCEuTb [Fig. 1(b)], we observed the characteristic absorption peaks of Eu^{3+} at ~393 and ~464 nm, which could be assigned to the $^7F_0 - {}^5L_6$ and $^5D_2$ transitions of Eu^{3+}, respectively, while the typical absorption of Tb^{3+} with peaks at 377 nm ($^7F_6 - {}^5D_3$) can also be observed in Tb^{3+}-doped samples. Moreover, the

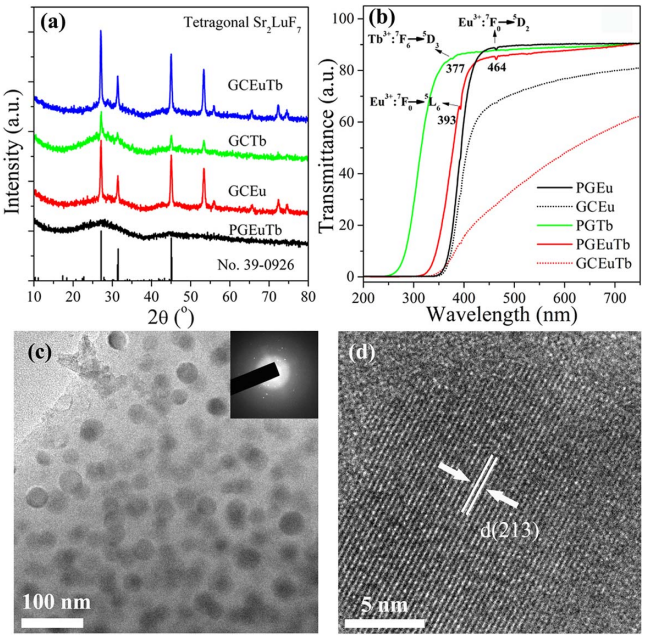

Fig. 1. (a) XRD patterns of PGEuTb, GCEu, GCTb, and GCEuTb and the standard data for Sr_2LuF_7 (JCPDS No. 39-0926); (b) transmission spectra of PGEu, GCEu, PGTb, PGEuTb, and GCEuTb; (c) TEM and (d) HRTEM images of nano-structured GCEu. The inset is corresponding SAED patterns.

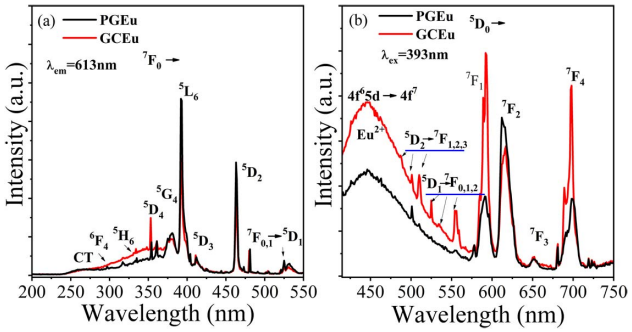

Fig. 2. (a) Excitation ($\lambda_{em} = 613$ nm) and (b) emission ($\lambda_{ex} = 393$ nm) spectra of PGEu and GCEu.

cut-off wavelength of GC shows a clear red shift compared to that of PG, which is due to the scattering effect of particles and further confirms the formation of Sr_2LuF_7 nano-crystals. Even so, the transparency of GC samples reaches 60% in the GCEuTb sample, which reveals the small size of the formed nano-particles.

To directly confirm the formation of Sr_2LuF_7 nano-crystals, the TEM and high resolution TEM (HRTEM) images of GCEu samples were measured, as shown in Figs. 1(c) and 1(d), respectively. From the TEM image displayed in Fig. 1(c), it is very clear to see dark uniform nano-crystals on the amorphous glass matrix, which directly reveal the crystallization of Sr_2LuF_7 in alumino-silicate glasses. It is worth mentioning that the formed Sr_2LuF_7 nano-crystals are homogeneous in grain size (~26 nm), which is consistent with results from XRD patterns. With the suitable crystalline size to this glass matrix, the glass samples of both PGEu and GCEu show high transparency[35] of up to 72%. The corresponding selected area electron diffraction (SAED) patterns of the GCEu sample, as presented in Fig. 1(c), reveal the polycrystalline feature of Sr_2LuF_7 nano-crystals, suggesting this hybrid optical material is composed of poly-nano-crystals and amorphous alumino-silicate glasses. Besides, as presented in Fig. 1(d), the lattice structure can be observed in the HRTEM image. The interplanar spacing d from HRTEM is ~3.330 Å, which can be attributed to (213) of tetragonal Sr_2LuF_7 ($d_{(213)} = 3.284$ Å).

After detailed structural characterizations, the optical properties of Sr_2LuF_7 glass-ceramics were investigated. As shown in the excitation ($\lambda_{em} = 613$ nm) spectra [Fig. 2(a)], characteristic excitation features (350–550 nm) of Eu^{3+} are observed in GCEu, which can be attributed to $4f - 4f$ transitions of Eu^{3+} ions[35–38]. The excitation peak at 393 nm should be from the $^7F_0 \rightarrow {}^5L_6$ transition of Eu^{3+}. The emission ($\lambda_{ex} = 393$ nm) spectra [Fig. 2(b)] show typical red and green emission peaks from $^5D_0 \rightarrow {}^7F_J$ ($J = 0$–4) and $^5D_1 \rightarrow {}^7F_J$ ($J = 1$–3) transitions of Eu^{3+} ions (500–720 nm), respectively. Compared to PGEu, the 613 nm and 702 nm emissions of Eu^{3+} ions of GCEu are highly improved after thermal treatment. Furthermore, Stark splitting for $^5D_1 \rightarrow {}^7F_1/{}^7F_2$ transitions of Eu^{3+} ions is observed after crystallization. These phenomena suggest the successful enrichment of Eu^{3+} into Sr_2LuF_7 nano-crystals. Moreover, the broadband excitation and emission of Eu^{2+} were also observed in Sr_2LuF_7 glass-ceramics, which will be discussed in detail in the following.

As is known to us, the intensity ratio R of $^5D_0 \rightarrow {}^7F_2$ to $^5D_0 \rightarrow {}^7F_1$ emissions is recognized as a sensitive probe to evaluate the symmetry of the local crystal field around Eu^{3+}. A low value of R reveals high symmetry of the surrounding environment[19–21,35,36,39]. Here, the R is decreased from 2.04 (PGEu) to 0.96 (GCEu), which suggests the enrichment of Eu^{3+} into formed Sr_2LuF_7 nano-crystals with higher symmetry.

Furthermore, the broadband emission of Eu^{2+} ($4f^65d \rightarrow 4f^7$ transition)[34,35], which is centered at about 450 nm, is also observed in both PGEu and GCEu, suggesting Eu^{2+} and Eu^{3+} co-exist in the hybrid materials, and partial Eu^{3+} is reduced to Eu^{2+} during melting-quenching, considering the raw material of EuF_3. Figure 3(a) illustrates the typical emission of Eu^{2+} in PGEu and GCEu samples upon the excitation of 350 nm. Compared with PGEu, the broadband Eu^{2+} emission in GCEu is enhanced obviously after the crystallization of Sr_2LuF_7 nano-crystals. In addition, the emission peak at 422 nm in PGEu presents a red shift to 430 nm in GCEu after crystallization, which is caused by the strong vibration around $Eu^{2+} - Eu^{2+}$ ions with a shortened distance. Figures 3(b) and 3(c) show the normalized typical emission and excitation spectra in the

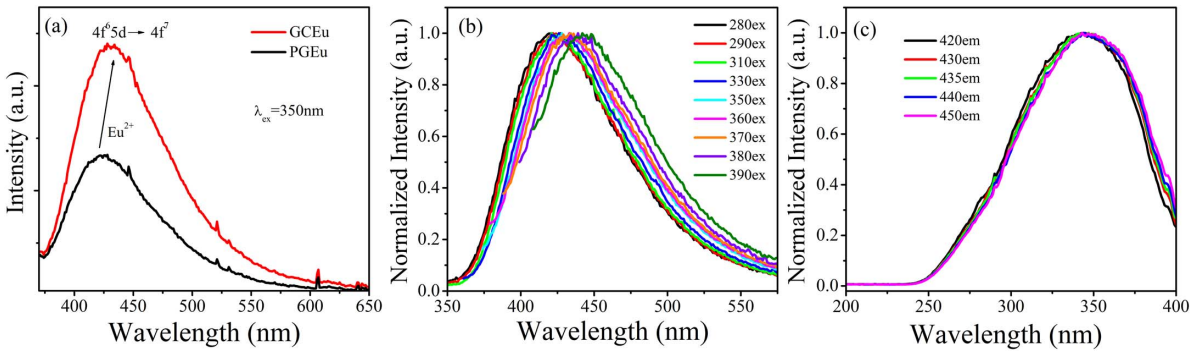

Fig. 3. (a) Emission spectra of PGEu and GCEu excited by 350 nm; normalized (b) emission and (c) excitation spectra of Eu^{2+} ions in the GCEu sample.

GCEu sample. Clearly, the emission peak shows an obvious red shift from 420 to 445 nm with an increase in the excitation wavelength from 280 to 390 nm. Simultaneously, the emission color of glass-ceramics is tunable from bluish violet to blue, as shown in following Commission International de l'Eclairage (CIE) figure. This broadband and color-tunable emission of Eu^{2+} ions in the stable GCEu sample could be a potential candidate for a UV pumped light source, such as a lamp for plants.

The conversion of Eu^{3+} to Eu^{2+} in air atmosphere may be understood by two models[40,41]: one is the reduction caused by volatilization of fluoride, and the other one is the charge compensation model. For the former, Eu^{3+} is reduced in the melting process, with the volatilization of fluoride: $2Eu^{3+} + 2F^- \rightarrow 2Eu^{2+} + F_2\uparrow$, which corresponds to the existence of Eu^{2+} emission in the PGEu sample [shown in Fig. 2(b)]. For the latter, when doped into Sr_2LuF_7 nano-crystals, Eu^{3+} will replace Sr^{2+}(1.18 Å) ions. At the same time, two Eu^{3+} ions are essential to substituting three Sr^{2+} ions, so as to keep the charge balance. As a result, two defects $[Eu^{\cdot}_{Sr}]$ and one cation vacancy $[V''_{Sr}]$ would be created simultaneously. Here, $Eu^{\cdot}_{Sr}$ presents one positive charge, while V''_{Sr} holds two negative charges. V''_{Sr} is a donor of electron, while $Eu^{\cdot}_{Sr}$ acts as the acceptor. Via thermal treatment, the electrons in V''_{Sr} are released and then trapped by $Eu^{\cdot}_{Sr}$, finally resulting in the reduction of Eu^{3+}. This charge compensation model can well illustrate the enhanced emissions of Eu^{2+} in Figs. 2(b) and 3(a).

Figure 4 shows the excitation ($\lambda_{em} = 543$ nm) and emission ($\lambda_{ex} = 377$ nm) spectra of GCEuTb and GCTb. By monitoring the $^5D_4 \rightarrow {}^7F_5$ emission for Tb^{3+} at 543 nm, typical excitation peaks at 283, 302, 316, 340, 350, 368, 377, and 483 nm are observed, and they can be attributed to $^7F_6 \rightarrow {}^5I_8$, $^5H_6$, $^5H_7$, $^5L_7$, $^5L_9$, $^5D_2$, $^5D_3$, and $^5D_4$ transitions for Tb^{3+}, respectively[13]. As presented in Fig. 4(b), upon the excitation of 377 nm ($^7F_6 \rightarrow {}^5D_3$) light, emission bands with peaks at 488, 543, 585, and 621 nm can be observed, which are attributed to $^5D_4 \rightarrow {}^7F_J$ ($J = 6$–3) of Tb^{3+}, respectively. Bright green emissions of the GCTb sample can be obtained when excited by 377 nm.

The emission intensity is highly enhanced with Tb/Eu co-doping on account of the energy transfer (ET) from

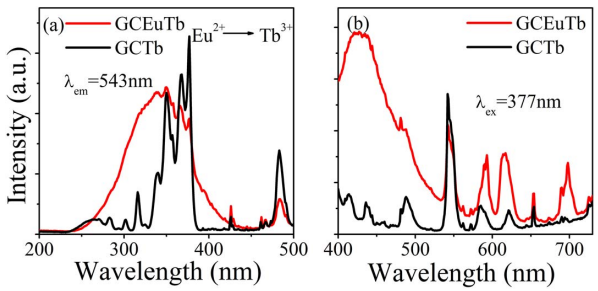

Fig. 4. (a) Excitation ($\lambda_{em} = 543$ nm) and (b) emission ($\lambda_{ex} = 377$ nm) spectra of Tb^{3+}-doped samples (PGTb and GCTb).

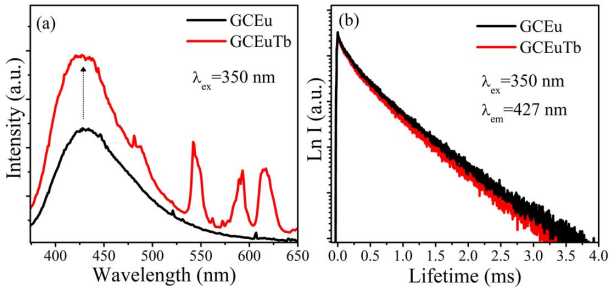

Fig. 5. (a) Emission spectra ($\lambda_{ex} = 350$ nm) and (b) decay lifetime of Eu^{2+} ions ($\lambda_{ex} = 350$ nm, $\lambda_{em} = 427$ nm) of GCEu and GCEuTb samples.

Eu^{2+} to Tb^{3+}. The ET is relatively apparent when excited by 350 nm, which can be certified by the decay lifetimes[25] of Eu^{2+} ions in GCEu and GCEuTb samples [Fig. 5(b)]. The lifetime of Eu^{2+} in the GCEu sample was about 838 μs, while that in GCEuTb was slightly reduced by 52 μs. Simultaneously, as is shown in Fig. 5(a), when excited by 350 nm, the Eu^{2+} emission is enhanced in GCEuTb due to better crystallization and larger crystallization size of Sr_2LuF_7 nano-crystals, which means the phonon energy around Eu^{2+} is further lowered. This phenomenon is in accordance with the sharper diffraction peaks of GCEuTb than GCEu in XRD patterns in Fig. 1.

Besides, as mentioned in Fig. 3, when excited by different excitation wavelengths, these glass-ceramics can exhibit tunable color from bluish violet to blue. Figure 6 shows the CIE of the GCEu sample excited by 280, 300, 350, and 393 nm, respectively. Simultaneously, the green emission of Tb^{3+} can be also obtained in the GCTb sample excited by 377 nm, as presented in Fig. 6. Combined with the blue (Eu^{2+}), green (Tb^{3+}), and red (Eu^{3+}) emission, near white emission can be expected under UV excitation in Eu/Tb co-doped Sr_2LuF_7 glass-ceramics. This indicates that Eu/Tb co-doped Sr_2LuF_7 glass-ceramics have potential application in WLED fields.

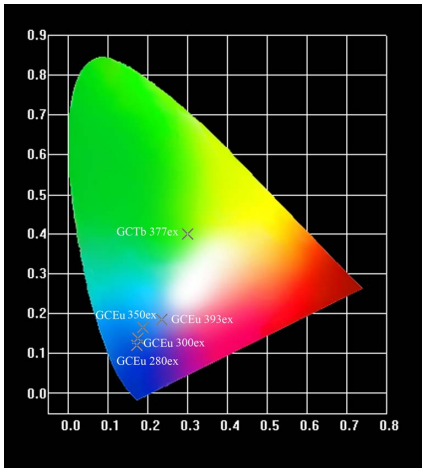

Fig. 6. CIE of GCEu (excited by 280, 300, 350, and 393 nm) and GCTb (excited by 377 nm).

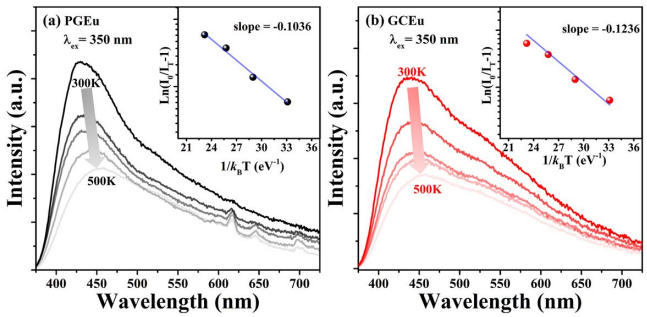

Fig. 7. Emission spectra excited by 350 nm of (a) PGEu and (b) GCEu under different temperatures from 300 to 500 K.

As known to us, thermal quenching performance is vital for the application of glass and glass-ceramics as light sources[12,42,43], especially for long-term use. The temperature-dependent photoemission spectra of Eu-doped glass and glass-ceramics were recorded to evaluate the quenching behavior. Under 350 nm excitation, the emission spectra of PGEu and GCEu within the range of 300–500 K were obtained and are presented in Figs. 7(a) and 7(b). Clearly, the emission intensities decrease gradually with elevation of the surrounding temperature. The emission intensities in PGEu and GCEu at 500 K are 56% and 52% of the initial intensity at 300 K, respectively. Due to the weakened emission of Eu^{3+}, here, the considered emission intensity is referred to as the whole integrated emission intensity from 375 to 725 nm of both Eu^{2+} and Eu^{3+}.

Generally, the thermal quenching behavior is caused by thermally activated multi-phonon non-radiative transition and is determined by activation energy (ΔE_a). The thermally activated non-radiative transition rate $k_{\rm nr}$ can be written as[44,45]

$$k_{\rm nr} = s\exp(-\Delta E_a/k_B T), \tag{2}$$

where s stands for frequency factor, k_B stands for the Boltzmann constant, and T stands for temperature. The ΔE_a can be obtained via the Arrhenius equation[45,46]:

$$I_T = \frac{I_0}{1 + C\exp(-\Delta E_a/k_B T)}, \tag{3}$$

where I_0 stands for the initial emission intensity, I_T stands for the integral emission intensity at T, and C is a constant. Based on Fig. 7, the values of ΔE_a for the emissions of Eu ions in PGEu and GCEu are obtained to be ~0.1036 and 0.1236 eV, respectively, which suggests PGEu presents a rapid degradation compared with GCEu, and GC shows better stability upon heating[47]. Moreover, ΔE_a was increased by 19.3% in this oxyfluoride Sr_2LuF_7 GC compared with that in oxyfluoride PG, which is conspicuously larger than that in Eu-doped phospho-alumino-silicate glass-ceramics containing $Ba_3AlO_3PO_4$ nano-crystals with the increased percentage of 1.8%[48]. These results indicate oxyfluoride Sr_2LuF_7 glass-ceramics not only show better thermal stability than PG, but also better improvement in thermal stability after crystallization than oxide glass-ceramics, such as $Ba_3AlO_3PO_4$ glass-ceramics, which endows these oxyfluoride glass-ceramics to be good candidates for WLEDs.

Dual valence Eu-doped tetragonal Sr_2LuF_7 glass-ceramics were fabricated via the melting-quenching method. Detailed structural characterizations including XRD, TEM, and HRTEM suggest the formation of novel Sr_2LuF_7 nano-crystals. The enhanced photoemission, prolonged decay lifetime, and Stark splitting reveal the enrichment of rare ions into Sr_2LuF_7 nano-crystals protected by an alumino-silicate glass network. We found that Eu^{3+}, Eu^{2+}, and Tb^{3+} co-exist in these hybrid materials, resulting in highly tunable blue–green photoemission. With the combination of broad blue–green emission of Eu^{2+}, green emission of Tb^{3+}, and sharp orange–red emission of Eu^{3+}, white light emissions can be achieved as excited by proper UV light. Furthermore, the construction of GC favors the improvement of glass thermal stability and makes it promising as a stable light source in practice. These results indicate that such novel Eu/Tb-doped transparent Sr_2LuF_7 glass-ceramics present potential applications in tunable light sources for display or lighting.

This work was supported by the National Natural Science Foundation of China (Nos. 51902178, 11804188, 51702172, and 51802285), the Natural Science Foundation of Shandong Province (No. ZR201807060932), and the Open Fund of the State Key Laboratory of Luminescent Materials and Devices (South China University of Technology) (No. 2019-skllmd-15).

References

1. E. F. Schubert and J. K. Kim, Science **308**, 1274 (2005).
2. P. Smet, A. Parmentier, and D. Poelman, J. Electrochem. Soc. **158**, R37 (2011).
3. D. Chen, Y. Yu, H. Lin, P. Huang, F. Weng, Z. Shan, and Y. Wang, Opt. Lett. **34**, 2882 (2009).
4. B. Zhu, S. Zhang, S. Zhou, N. Jiang, and J. Qiu, Opt. Lett. **32**, 653 (2007).
5. Q. Zhou, L. Dolgov, A. M. Srivastava, L. Zhou, Z. Wang, J. Shi, M. D. Dramićanin, M. G. Brik, and M. Wu, J. Mater. Chem. C **6**, 2652 (2018).
6. R. Wei, L. Wang, P. Zheng, H. Zeng, G. Pan, H. Zhang, P. Liang, T. Zhou, and R. Xie, J. Eur. Ceram. Soc. **39**, 1909 (2019).
7. Y. Qi, L. Zhao, W. Bian, X. Yu, X. Xu, and J. Qiu, Chin. Opt. Lett. **15**, 081601 (2017).
8. Y. Narukawa, I. Niki, K. Izuno, M. Yamada, Y. Murazaki, and T. Mukai, Jpn. J. Appl. Phys., Part 2 **41**, L371 (2002).
9. X. Piao, T. Horikawa, H. Hanzawa, and K. I. MacHida, Appl. Phys. Lett. **88**, 161908 (2006).
10. H. Lin, T. Hu, Y. Cheng, M. Chen, and Y. Wang, Laser Photon. Rev. **12**, 1700344 (2018).
11. O. G. Giraldo, M. Fei, R. F. Wei, L. Teng, Z. Zheng, and H. Guo, J. Lumin. **219**, 116918 (2020).
12. X. Liu, H. Guo, S. Dai, M. Peng, and Q. Zhang, Opt. Mater. Express **6**, 3574 (2016).

13. Z. Lin, X. Liang, Y. Ou, C. Fan, S. Yuan, H. Zeng, and G. Chen, J. Alloys Compd. **496**, L33 (2010).
14. M. Kemere, U. Rogulis, and J. Sperga, J. Alloys Compd. **735**, 1253 (2018).
15. X. Liu, J. Zhou, S. Zhou, Y. Yue, and J. Qiu, Prog. Mater. Sci. **97**, 38 (2018).
16. J. Cao, H. Guo, F. Hu, L. Li, S. Xu, and M. Peng, J. Am. Ceram. Soc. **101**, 3890 (2018).
17. R. Zhang, H. Lin, Y. Yu, D. Chen, J. Xu, and Y. Wang, Laser Photon. Rev. **8**, 158 (2014).
18. S. Yi, W. J. Chung, and J. Heo, J. Am. Ceram. Soc. **97**, 342 (2014).
19. G. J. Gao, N. Da, S. Reibstein, and L. Wondraczek, Opt. Express **18**, A575 (2010).
20. G. Gao, S. Reibstein, M. Peng, and L. Wondraczek, J. Mater. Chem. **21**, 3156 (2011).
21. G. Gao and L. Wondraczek, Opt. Mater. Express **4**, 476 (2014).
22. D. Chen, Y. Yu, P. Huang, H. Lin, Z. Shan, and Y. Wang, Acta Mater. **58**, 3035 (2010).
23. Q. Luo, X. Qiao, X. Fan, H. Yang, X. Zhang, S. Cui, L. Wang, and G. Wang, J. Appl. Phys. **105**, 043506 (2009).
24. H. Guo, F. Li, R. Wei, H. Zhang, and C. Ma, J. Am. Ceram. Soc. **95**, 1178 (2012).
25. H. Guo, R. F. Wei, and X. Y. Liu, Opt. Lett. **37**, 1670 (2012).
26. H. Guo, X. Wang, J. Chen, and F. Li, Opt. Express **18**, 18900 (2010).
27. Q. Zheng, Y. Li, W. Wu, J. Zou, B. Yang, and M. Shi, Chin. Opt. Lett. **17**, 101601 (2019).
28. S. Ouyang, W. Zhang, Z. Zhang, Y. Zhang, and H. Xia, Chin. Opt. Lett. **13**, 091601 (2015).
29. S. Wang, J. Chen, J. Lin, C. Yang, F. Huang, and D. Chen, J. Mater. Chem. C **7**, 14571 (2019).
30. J. Chen, Y. Peng, X. Li, W. Chen, H. Huang, L. Lin, and D. Chen, J. Mater. Chem. C **7**, 4109 (2019).
31. X. Li, D. Chen, F. Huang, G. Chang, J. Zhao, X. Qiao, X. Xu, J. Du, and M. Yin, Laser Photon. Rev. **12**, 1800030 (2018).
32. J. Zhong, D. Chen, Y. Peng, Y. Lu, X. Chen, X. Li, and Z. Ji, J. Alloys Compd. **763**, 34 (2018).
33. P. Chen, Y. Mao, S. Hou, Y. Chen, X. Liu, Y. Lou, A. Chen, L. Yang, J. Li, and N. Dai, Ceram. Int. **45**, 233 (2019).
34. H. Guo, X. Liu, F. Li, R. Wei, Y. Wei, and C. Ma, J. Electrochem. Soc. **159**, J223 (2012).
35. X. Liu, Y. Wei, and H. Guo, J. Am. Ceram. Soc. **96**, 369 (2013).
36. X. Liu, Y. Wei, R. Wei, J. Yang, and H. Guo, J. Am. Ceram. Soc. **96**, 798 (2013).
37. X. Li, H. Guo, X. Liu, R. Wei, F. Hu, and S. Zhou, J. Am. Ceram. Soc. **102**, 6640 (2019).
38. R. Wei, J. Guo, K. Li, L. Yang, X. Tian, X. Li, F. Hu, and H. Guo, J. Lumin. **216**, 116737 (2019).
39. D. Chen, Y. Wang, N. Yu, and P. Huang, J. Phys. Chem. C **112**, 18943 (2008).
40. M. Peng, Z. Pei, G. Hong, and Q. Su, J. Mater. Chem. **13**, 1202 (2003).
41. Q. Luo, X. Fan, X. Qiao, H. Yang, M. Wang, and X. Zhang, J. Am. Ceram. Soc. **92**, 942 (2009).
42. X. Zhang, L. Huang, F. Pan, M. Wu, J. Wang, Y. Chen, and Q. Su, ACS Appl. Mater. Interfaces **6**, 2709 (2014).
43. Z. Xia, Z. Xu, M. Chen, and Q. Liu, Dalton Trans. **45**, 11214 (2016).
44. J. Li, J. Yan, D. Wen, W. Khan, J. Shi, M. Wu, Q. Su, and P. Tanner, J. Mater. Chem. C **4**, 8611 (2016).
45. S. Saha, S. Das, U. K. Ghorai, N. Mazumder, D. Ganguly, and K. K. Chattopadhyay, J. Phys. Chem. C **119**, 16824 (2015).
46. K. J. Laidler, J. Chem. Educ. **61**, 494 (1984).
47. R. D. Shannon, Acta Crystallogr. A **32**, 751 (1976).
48. X. Li, D. Xu, X. Liu, and H. Guo, RSC Adv. **7**, 53839 (2017).